LA-UR- 10- 01310

Title:	Precursor Detonation Wave Development in ANFO due to Aluminum Confinement
Author(s):	Scott I. Jackson, Charles B. Kiyanda, Mark Short
Intended for:	14th International Detonation Symposium, Coeur d'Alene, Idaho, April 11-16, 2009

Los Alamos
NATIONAL LABORATORY
——— EST. 1943 ———

Form 836 (7/06)

Precursor Detonation Wave Development in ANFO due to Aluminum Confinement

Scott I. Jackson, Charles B. Kiyanda, and Mark Short

Shock and Detonation Physics Group

Los Alamos National Laboratory

Abstract. Detonations in explosive mixtures of ammonium-nitrate-fuel-oil (ANFO) confined by aluminum allow for transport of detonation energy ahead of the detonation front due to the aluminum sound speed exceeding the detonation velocity. The net effect of this energy transport on the detonation is unclear. It could enhance the detonation by precompressing the explosive near the wall. Alternatively, it could decrease the explosive performance by crushing porosity required for initiation by shock compression or destroying confinement ahead of the detonation. At present, these phenomena are not well understood. But with slowly detonating, non-ideal high explosive (NIHE) systems becoming increasing prevalent, proper understanding and prediction of the performance of these metal-confined NIHE systems is desirable. Experiments are discussed that measured the effect of this ANFO detonation energy transported upstream of the front by a 76-mm-inner-diameter aluminum confining tube. Detonation velocity, detonation-front shape, and aluminum response are recorded as a function of confiner wall thickness and length. Detonation shape profiles display little curvature near the confining surface, which is attributed to energy transported upstream modifying the flow. Average detonation velocities were seen to increase with increasing confiner thickness, while wavefront curvature decreased due to the stiffer, subsonic confinement. Significant radial sidewall tube motion was observed immediately ahead of the detonation. Axial motion was also detected, which interfered with the front shape measurements in some cases. It was concluded that the confiner was able to transport energy ahead of the detonation and that this transport has a definite effect on the detonation by modifying its characteristic shape.

Introduction

Accurate prediction of non-ideal high explosive (NIHE) detonation has become a topic of significant interest in recent years. Non-ideal explosives differ from conventional explosives in that they are usually high-porosity, low-density materials where the fuel and oxidizer are not mixed on a molecular level. As a result, NIHEs typically exhibit low detonation velocities. They also have much larger detonation reaction zones that are centimeters in length, rather than the 100's of microns associated with more ideal explosives.

The detonation velocities observed for many NIHEs are typically below the sound speeds of stiff confining materials, including common metals. This is in contrast to ideal high explosives (HEs), where the detonation velocity exceeds the sound speed of most confiners. In these ideal HE systems,

the detonation drives a shock into the inert confiner and no information propagation in the confiner exceeds the detonation velocity. The confiner is only able to influence the detonation by acting on the reaction zone behind the detonation shock and ahead of the sonic surface. Since the confiner is shocked and ideal HEs have small reaction zones, this implies that increasing the confiner thickness above a few reaction zone lengths has no effect on the detonation velocity.

In low-detonation-velocity, stiffly confined systems, no inert shock typically exists in the confinement since the confiner sound speed exceeds the detonation velocity. In fact, the confiner is actually able to transport energy from behind the detonation shock upstream to the unreacted explosive. This energy transmission can both enhance and hinder the detonation by modifying the amount of confinement it experiences. In some cases, this "precursor energy" will drive the confiner surface into the NIHE, compressing it. The precompression can densify the NIHE, increasing its detonation velocity[5], or even igniting it. However, precompression can also crush porosity out of the NIHE, desensitizing it and leading to detonation failure. The precursor energy can also cause loss of confinement ahead of the detonation, which can also result in detonation failure[1]. Finally, the large reaction zone lengths of NIHEs coupled with the subsonic confinement allow for a much greater dependence of confiner thickness on detonation velocity[7].

These types of wall-explosive phenomena are not typically present in most HE configurations. Our current level of physical understanding of this interaction prevents accurate modeling of confined NIHE systems. We seek calibration data for the Detonation Shock Dynamics (DSD) code to resolve this limitation. DSD is able to model detonation propagation when supplied with two parameters: the detonation velocity variation versus detonation surface curvature and the detonation edge angle at the explosive-confiner interface. The velocity-curvature relationship is derived from experimental rate-stick data. For ideal HEs, the edge angle is found from shock polar analysis[3, 2]. However, since the confiner flow is shockless and subsonic in NIHEs when the confiner sound speed exceeds the detonation velocity, alternate methods must be

implemented. Experimental measurements are required for the development of these new techniques.

In this work, we experimentally characterize the interactions between the detonation front, a stiff confiner, and the unreacted explosive. Ammonium-nitrate-fuel-oil (ANFO) was selected as the NIHE and aluminum tubes were used as confiners. Experimentally observed ANFO detonation velocities range from 1.5–4.0 mm/μs depending on the explosive properties, charge size and degree of confinement[4], while the longitudinal sound speed of aluminum is in excess of 5.0 mm/μs. Parameters include the confiner wall thickness and detonation run length. We measure the detonation wave speed as well as the velocity and relative strength of the elastic stress wave that is driven in the metal ahead of the detonation. Detonation front profiles are also recorded at the end of the tube. Our intent was to identify regimes where the detonation was dramatically affected by this interaction.

Experiment

Three separate experimental configurations were fielded. Our methodology was first to determine the required booster strength to detonate aluminum-confined ANFO; secondly, to obtain front shape and velocity data; and finally, to measure the motion of the confiner during the experiment. All tests used 76-mm-inner-diameter tubes filled with ANFO mixtures consisting of 94% ammonium nitrate prills by weight mixed with 6% No. 2 diesel fuel by weight. Porous, industrial-grade ammonium nitrate was used from Dyno Nobel with a typical bulk density of 0.80 g/cc with the average prill diameter ranging from 1.4–2.0 mm. Mixing was accomplished by combining the prills and diesel fuel in a cement mixer and mixing for a minimum of 15 minutes. ANFO was then poured into each tube in 200-g increments. Each incremental fill was hand-tamped to prevent significant clumping or void formation. This methodology was sufficient to achieve an ANFO density of 0.86–00.90 g/cc.

Booster-Strength Evaluation

A series of tests were performed to determine the appropriate strength booster for use in the aluminum experiments. Due to the short aspect ra-

tio of the aluminum-confined experiments, which had length-to-inner-diameter (L/D) ratios of 4 and 12, it was essential to promptly initiate detonation without significant overdrive. Little data was available to assist in booster selection. Primasheet 1000, a flexible rubberized explosive composed of 63% PETN, 8% nitrocellulose, and 27% plasticizer, was chosen as the booster explosive due to its availability and ease of machining. Shocks driven by detonating Primasheet into ANFO were of sufficient strength to induce chemical reactions; in question was the booster thickness necessary to support the shock long enough for these reactions to complete and support detonation.

As a conservative measure, PVC tubing was used as the confining material for these scoping experiments, as a booster sufficient to initiate PVC-confined ANFO would also initiate ANFO surrounded by a stiffer aluminum tube. Lengths of PVC tubing that had a 305-mm length, 76-mm ID, and 6.35-mm-thick wall were filled with ANFO. The downstream end of each tube was sealed with a 6061-aluminum witness plate, the deformation of which provided a rapid and inexpensive diagnostic to evaluate the relative strength of the detonation. The upstream end contained a 76-mm booster explosive backed by 12.7-mm of polycarbonate. Booster thicknesses and the resulting witness plate data are given in Tab. 1.

temper, except for the 25.4-mm-thick tubing, which was T6511. The downstream end of each tube was sealed with a 6.35-mm-ID PMMA window with an outer diameter matching that of the tube (Fig. 1). A centerline on the window contained a line of PETN paint backed by 80-μm-thick copper tape (Fig. 2). Arrival of the detonation shock at this location initiated the PETN with a bright flash that was recorded by a streak camera, yielding the front shape record.
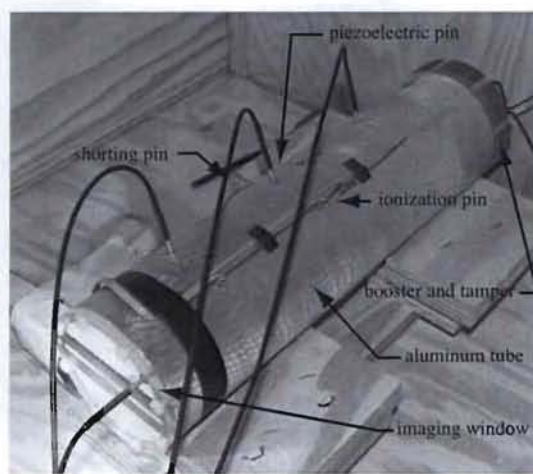

Fig. 1. The tube from test 6-305.

Table 1. Booster information and results.

Primasheet Thickness (mm)	Dent Depth (mm)	Prill Diameter (mm)
3	2.0	39.4
4	2.8	46.7
5	3.5	50.8
6	8.5	76.2

Pin Data and Front-Shape Records

Aluminum tubes were used to confine the ANFO during the front shape measurements. Each tube was 76.2 mm in ID. Wall thickness ranged from 6.35–25.4 mm and the tube lengths were 305 or 914 mm (Tab. 2). All were 6061 alloy and T6
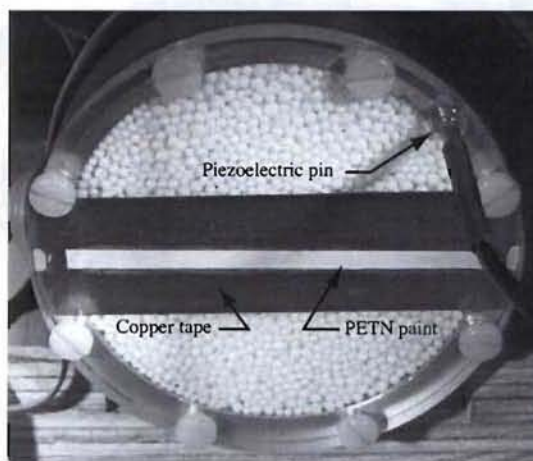

Fig. 2. The downstream end window of the 6.35-mm-thick, 305-mm-long tube filled with ANFO.

Each aluminum tube also contained three types of diagnostic pins to detect the transit of various waves. These pins were mounted in the wall to be flush with the tube ID. Dynasen ionization (CA-1040) and shorting pins (CA-1038) pins were used to measure the ion and shock arrival, while tightly fitted piezoelectric pins (CA-1136) recorded both compression of the tube wall, to detect the precursor stress wave in the aluminum, as well as the arrival of the detonation. The piezoelectric pins could only be used for relative pressure measurements as they were not calibrated and were being used as a combined wall-stress gauge and ANFO pressure transducer. Pins were located 93.1-mm axially apart and were spaced apart 45° deg radially (Fig. 3). A piezoelectric pin was also located in the end window against the downstream tube surface. Detonation initiation was accomplished with 12.7-mm-thick Primasheet 1000 booster and an RP-1 detonator, tamped from behind by 12.7-mm of polycarbonate. All pins were sampled at 1.25 GHz. This sample rate coupled with the pin spacing provided velocity uncertainties of 1% for the ionization and shorting pins, and 3% for the piezoelectric pins.
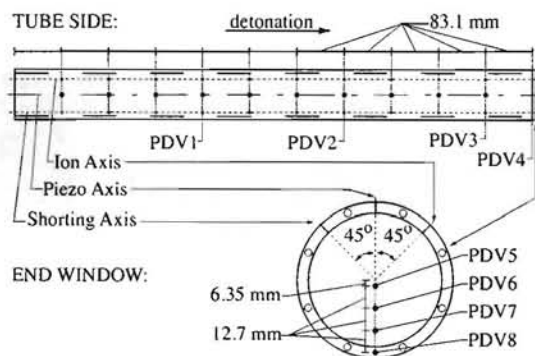

Fig. 3. A schematic of the pin and probe locations on the 6.35-mm-thick, 914-mm-long tube.

PDV-instrumented Test

Photon-Doppler Velocimetry (PDV), a light-based interferometry technique[6], was used to obtain the tube wall velocity during test 12-914. Four focused probes (PDV1–PDV4) were mounted along the sidewall of the tube and four collimated probes (PDV5–PDV8) were stationed in a radial line along the end window (Fig. 3). All probes were both orthogonal to and spaced 50 mm from the imaging surface. End-wall probes imaged the inner surface of the window, which was sanded with 100-grit sandpaper and then covered with copper tape to ensure optimum reflectance.

Results and Discussion

Booster-Strength Analysis

The results of the booster-strength tests are shown in Tab. 1. The dent depth measurement is the maximum depression located at the center of the witness plate, relative to the plate edges that were not exposed to the explosive. The prill imprint measurement is the diameter of the region on the witness plate that was dimpled by the detonation shock driving the prills into the metal surface of the witness plate.

Both of these values continuously increased with increasing booster thickness. Of particular concern was the variation in prill imprint diameter, which was below the 76-mm tube ID for all boosters except the 6-mm case. This indicated that the detonation initiated by the 76-mm diameter booster was decaying due to expansion effects at the wall and that an annular region of the outer diameter was not detonating. Only with the thickest booster tested (6 mm) did the prill imprint diameter match that of the initial booster diameter, indicating no wave decay. The dent depth of 8.5 mm for this test also demonstrated a dramatic increase over previous values of 2–3.5 mm recording the arrival of a much more robust detonation at the witness plate.

Based on these measurements, it was inferred that a stable (or very slowly decaying) detonation was initiated in the 76-mm-diameter PVC tubing with the 6-mm booster. As a safety factor and to account for the possibility that steady state was not reached in the short length tested (L/D = 4), a booster thickness of 12 mm was selected for aluminum-confined tests. It was assumed that this increase in booster thickness, coupled with the increased confinement of the aluminum wall, would initiate a stable detonation with minimal overdrive. Pin measurements confirmed this assumption, as discussed below.
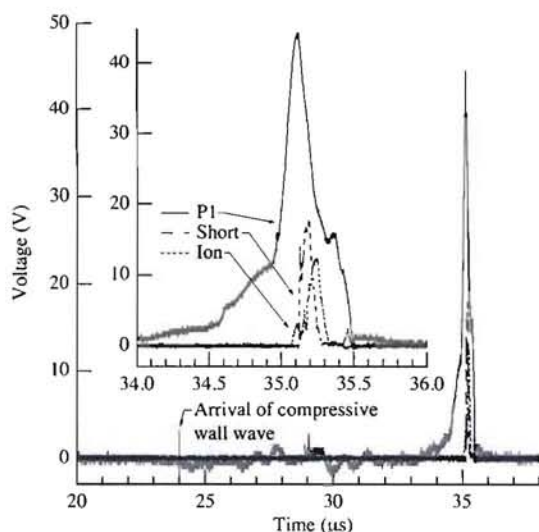
Fig. 4. Example of pin data traces.

Pin and Front-Shape Data

Pin Data: An example of the pin data from test 12-305 is shown in Fig.4. Early in time, at approximately 24 μs, the arrival of the precursor stress wave is detected by the piezoelectric pin, as denoted by an oscillating waveform of increasing strength. As the detonation front arrives at the pin station near 35 μs, the pin records substantially increased compression, followed by a rapid release that was likely due to pin failure. During the period of increased compression, both the ionization and shorting pins trigger within 100 ns of each other. In every test, all pins at each station triggered within 1 μs of each other. A pin was considered to have triggered when the signal rose above the bit noise associated with the data acquisition system. Additionally, there is a trigger delay inherent in the mechanical design of the shorting pin, which requires the shock pressure to move a brass cap across a 64-μm gap, while no such delay exists for either the piezoelectric or ionization pins. This may explain why the shorting pin triggers last.

Pin arrival times were recorded from each test and complied to form position-time plots of the wave motion in the experiment. An example of one such plot is shown in Fig. 5 for test 12-914. The progression of the detonation can be seen from the closely matched ionization, shorting and piezoelectric shock pin trigger times. The propagation of the elastic stress wave in the metal is also seen ahead of the detonation front. The data from each pin fit well to a line using a least squares fit, the slope of which yields the average wave velocity in the experiment.
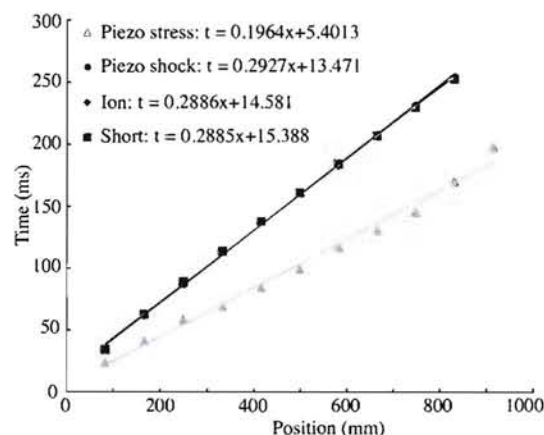

Fig. 5. Position-time diagram for the 12.7-mm-thick, 914-mm-long tube showing pin trigger times and average velocity fits. Ionization, shorting, and piezoelectric shock data are on top of each other.

These average wave velocity data are reported in Tab. 2. The velocity of the elastic precursor ranges from 5.1-6.5 mm/μs, which is consistent with the speed of sound in aluminum. Detonation velocities range from 2.7-3.6 mm/μs, increasing with wall thickness up to the maximum 25.4-mm wall thickness tested. As mentioned, this trend was expected due to the extended length of the ANFO reaction zone and the subsonic confinement condition. No inert shocks were present to limit the entire confiner thickness from acting on the reaction zone[7].

Overall, we find the agreement of the linear velocity fit to the elastic precursor wave data to be good, with squared correlation coefficients above 0.987. The fit to the detonation pin data is excellent, with all squared correlation coefficients above 0.996. The lower fit correlation for the elastic stress wave is attributed to multiple issues: The Primasheet booster overdrives the precursor wall wave initially, as evidenced by the higher elastic wave speeds in the shorter length tubes. Additionally, de-

Table 2. Dimensional and average velocity data. Asterisk (*) denotes the T6511 temper tube, all others were T6.

Test Name	Wall Thickness (mm)	Tube Length (mm)	Short Pin Shock U (mm/μs)	Ion Pin Shock U (mm/μs)	Piezo Pin Shock U (mm/μs)	Piezo Stress Wave U (mm/μs)
6-305	6.35	305	2.772	2.690	2.814	5.721
6-914	6.35	914	2.838	2.797	2.904	5.453
12-305	12.70	305	3.125	3.193	3.092	5.615
12-914	12.70	914	3.466	3.465	3.416	5.092
25-305	25.40	305	3.383	3.588	3.377	6.480*

tection of the elastic precursor signal can be difficult due to its low amplitude, which can be exacerbated by a poorly fit pin not sensing early compression due to insufficient sidewall contact.

The detonation, however, does not exhibit any overdrive associated with the initiation process. In fact, comparison tests of identical wall thicknesses find average velocities that are consistently 3-10% lower for the short tubes, relative to the longer lengths tested, indicating that the wave is slightly underdriven from the booster.

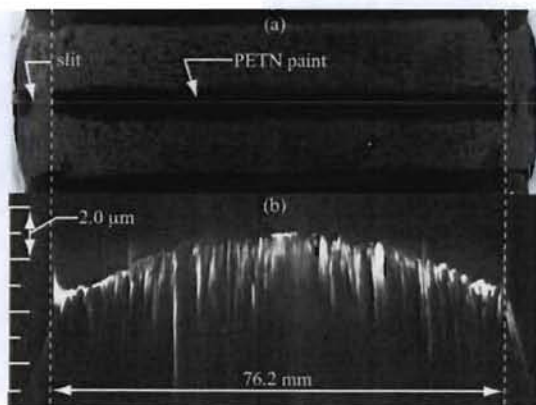*Front-Shape Records*: Figure 6 shows the front shape data for test 6-305. The upper image is a

Fig. 6. Still frame (a) and streak image (b) for 6.35-mm-thick, 305-mm-long tube.

still frame showing the imaging slit of the window in Fig. 2. The lower image is the streak data with time increasing downwards. The granular nature of the explosive is reflected in the streak and some jetting of product gas ahead of the main shock is also evident, particularly at the left wall. Such jetting is also observed in ANFO rate sticks with weaker confinement and is due to a gap at the wall allowing product gases to rush ahead of the main front. The gap is believed to be due to either the subsonic wall pulling away from the explosive ahead of the detonation or the absence of a prill near the wall on the imaging centerline. A more definitive conclusion is not possible in the current study and jets effects are neglected in the following curvature discussion.

The front shape profile shows low curvature near the tube center, indicating a locally higher propagation velocity in the region most isolated from wall expansion. Curvature increases with increasing diameter to a maximum between the tube center and the wall, and then decreases near the wall. Different behavior is observed in more weakly confined systems, such as Fig. 8 in Ref. [6]-REF[4], where the detonation curvature is at a minimum at the center and monotonically increases outwards towards the wall. Thus, the aluminum confiner is not only providing additional confinement, but also modifying the characteristic shape of the wavefront.

A compilation of all front shape measurements to date is shown in Fig. 7. All images are identically scaled. Similar features as discussed in Fig. 6 are seen in all traces. It is apparent that increasing the wall thickness not only increases the detonation velocity, but also results in a detonation profile with less overall curvature. Such behavior agrees well with theory[7]. Jetting aside, all fronts also appear fairly symmetric.

Comparison of the prominent front in each record (except Fig. 7b, where the fainter leading wave is used) shows little difference between the short- and long-length tubes for each wall thickness tested.
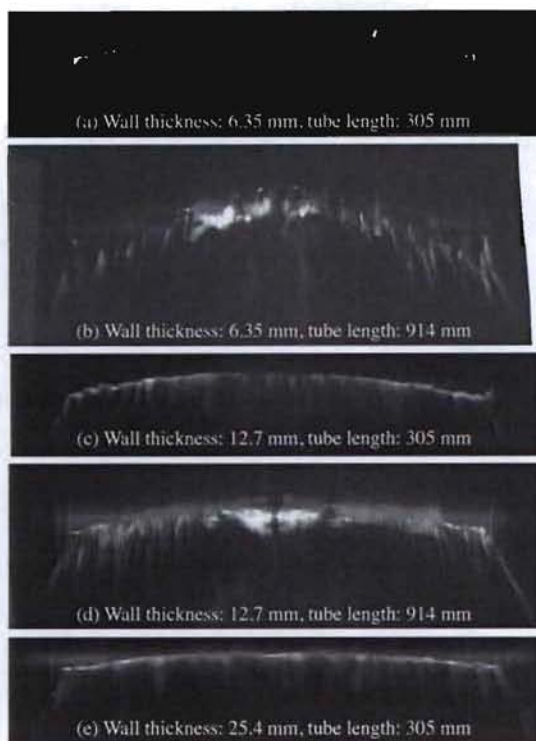
Fig. 7. Streak records.

Fig. 8. Sidewall velocity data from probe PDV3.

This indicates that the wave shape approaches its steady state rapidly (within $L/D = 4$). In some cases (b, d, and e in Fig. 7), the streak record shows two-wave structure, with a diffuse or weaker front arriving before the main front. Since the imaging section is PETN paint backed by copper tape, this indicates low-level PETN ignition followed by stronger reaction. This phenomenon is clarified by the PDV diagnostic results in the next section.

PDV Analysis

The following data was recorded for test 12-914, matching the position-time plot of Fig. 5.

Sidewall probes: An example of the PDV sidewall data for probe PDV3 is shown in Fig. 8. Starting near 150 μs, the arrival of the precursor wave induces early movement (inset) of up to 4 m/s first radially outwards then inwards. The arrival of the detonation shock near 250 μs then rapidly increases the wall velocity up to 1.0 mm/μs as the wall is
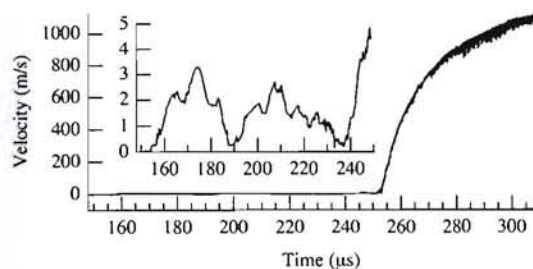
driven outwards by the expanding detonation products. Sharpe and Bdzil[7] predicted that the precursor motion would be first inwards, followed by outward motion due to the detonation arrival. This is similar to the current results but does not recover the initial inwards motion observed, which may be an initiation transient.

The other sidewall probes exhibit phenomenologically identical behavior and in all cases the precursor arrival times are consistent with the pin data. The detected radial motion from the precursor wave appears insufficient to noticeably precompress the ANFO near the wall. Furthermore, large-scale radial expansion, associated with the arrival of the detonation, commences 2.5 μs before the Dynasen pins detect the detonation. As only outer wall motion is measured, the response of the ANFO to this motion is unknown.

End window probes: The PDV window probe data is shown in Fig. 9. As shown in the inset, the arrival of the elastic wave induces early downstream motion of the end window, near 170 μs, almost 100 μs before the arrival of the detonation. The outer edge of the window starts motion earlier and moves 3.85 mm prior to that arrival of the detonation, while the center only moves 0.49 mm. The 3.36-mm difference in motion implies that the inner surface of the window is bending in a concave fashion.

The motion of the window during this 100-μs period is thought to separate the inner window surface from the ANFO. We deem it unlikely that the axial wall motion also moves the ANFO significantly downstream because: (1) The prills are not attached to the wall, so axial wall motion would transmit little shear force to the prills. (2) Any induced prill motion near the wall would be absorbed by the gran-
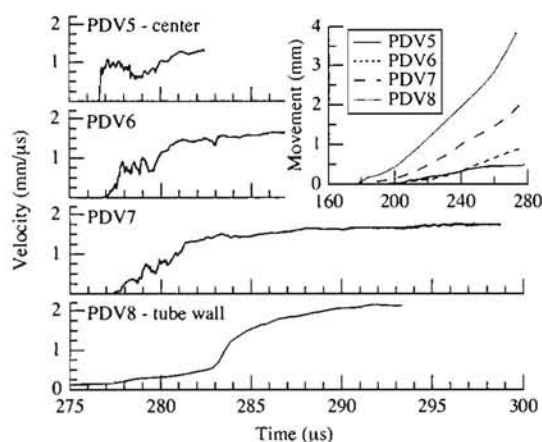
Fig. 9. Endwall PDV data.

ular nature of the explosive and would not propagate inwards. Thus, it is likely that an air gap exists between the prills and the inner window, whose width increases with radius and magnitude corresponds to the motion shown in the inset of Fig. 9.

A detonation encountering such a low-impedance gap would be transmitted as a shock and would reflect back and forth between the higher-impedance inner window and detonation products, effectively Òringing upÓ the window particle velocity until all materials had identical pressure and velocity conditions. The PDV data of the shock arrival at the window support this hypothesis. The center probe (PDV5) measures a sharp shock, consistent with a small gap. Probes PDV6 and PDV7 both exhibit ring-up behavior as indicated by the repeated small shocks that accelerate the window. The velocity signal from PDV7 rises more gradually than that of PDV6, which has a smaller gap that allows for shorter shock transit times.

At the PETN-flash, this ring-up behavior appears to manifest itself as two waves: a weak or diffuse ignition followed by a stronger reaction when the pressure driving the PETN reaction rises sufficiently during the ring-up. This effect is not window ghosting due to total internal reflection as all waves have curvature. Such double-wave structure is not observed in front shape records for the short tubes with 6.35-mm and 12.7-mm walls (Figs. 7a and 7c). It is present in the short 25.4-mm-wall test (Fig. 7e), but the first faint shock is almost on top of the stronger

wave. This is in contrast to the streak records from the longer tubes (Figs. 7b and 7d), which show substantial separation between the two waves. The separation between the arrival of the precursor wall wave and the detonation front at the end window is about 50 μs in the short tubes and 100 μs in the long ones. The increased time for window movement in the longer tubes supports the larger wave separation. Increasing the wall thickness also seems to increase the strength of the leading wave.

Besides imposing a second diffuse wave on the streak images, the presence of such a variable-width gap also artificially induces additional curvature on the front profile due to the time required for the air shock and detonation products to traverse the gap. In order to mitigate this effect, future tests will need to decouple the window from the tube wall motion in order to maintain contact at the explosive-window interface. A redesigned test is being implemented to accommodate this requirement. The redesigned measurement surface will also be positioned away from the downstream tube end to record the detonation shape prior to the arrival of the reflected elastic precursor at the measurement location.

Conclusion

Detonation waves were propagated in aluminum tubes filled with the non-ideal high explosive ANFO. Tube wall thickness varied from 6.35 to 25.4 mm while lengths of 305 and 914 mm were used. This configuration was of interest because the sound speed of the aluminum confiner exceeded the detonation velocity, preventing a shock from forming in the tube wall and allowing the aluminum to transport energy from behind the detonation front to the undisturbed explosive upstream. Preliminary boosting tests were also conducted to determine the wave strength required to initiate stable ANFO detonation without significant overdrive.

Front shape records showed maximum curvature away from the wall, with different characteristic wave shapes than observed in weakly confined ANFO. Detonation and aluminum stress wave velocities were recorded with shorting, ionization, and piezoelectric pins embedded in the tube wall. In all cases, increasing the tube wall thickness led to higher detonation velocities and less wavefront cur-

vature, as predicted by prior work[7]. Double shock structure was also observed in some tests and attributed to separation of the imaging window from the explosive.

Tube wall motion was recorded with PDV for the test of the 12.7-mm-thick, 914-mm-long tube. Energy transported ahead of the detonation resulted in weak (4 m/s) outward, then inward radial motion of the tube wall until a few microseconds before arrival of the detonation, at which point the tube rapidly expanded outwards, reaching 1 mm/μs. Axial motion of the downstream tube end prior to the arrival of the detonation was sufficient to arc the attached imaging window. This motion separated the window-explosive interface, creating a variable-width gap. The detonation transmitted across this gap as an air shock, partially igniting the PETN-flash. Increasing pressure due to subsequent shock ring-up eventually caused the window to fully flash. Such behavior is believed responsible for double-wave structure observed in some streak records and will need to be accounted for in the streak records. Longer periods of window motion and thicker tube walls allowed for increased energy transport ahead of the detonation and were seen to increase the double-wave spacing.

The velocity, front-shape, and PDV data collected are essential to understand and accurately model the behavior of low-detonation-velocity explosives in higher-sound-speed confiners. The booster strength and velocity data are also of interest to future experimental efforts involving ANFO, as little data are available for aluminum-confined ANFO at the longer lengths tested. Future tests will further explore the discussed phenomena in larger-diameter, longer-length tubes to verify the steady-state propagation behavior and obtain higher-fidelity front-shape measurements that are unaffected by the early wall motion.

Acknowledgements

References

1. Arai, H. , Ogata, Y. , Wada, Y. , Miyake, A. , Jung, W. , Nakamura, J. , and Ogawa, T. . Detonation Behavior of ANFO in Resin Tubes. *Sci. Technol. Energetic Mat.*, 65:201–205, 2004.

2. Aslam, T. and Bdzil, J. . Numerical and Theoretical Investigations on Detonation-Inert Confinement INteractions. In *Proceedings of the 12th International Symposium on Detonation*, pages 483–488. Office of Naval Research, 2002.

3. Aslam, T. and Bdzil, J. . Numerical and Theoretical Investigations on Detonation Confinement Sandwich Tests. In *Proceedings of the 13th International Symposium on Detonation*, pages 761–769. Office of Naval Research, 2006.

4. Bdzil, J. , Aslam, T. , Catanach, R. , Hill, L. , and Short, M. . DSD Front Models: Nonideal Explosive Detonation in ANFO. In *Proceedings of the 12th International Symposium on Detonation*, pages 409–417. Office of Naval Research, 2002.

5. Eden, G. and Belcher, R. . The Effects of Inert Walls on the Velocity of Detonation in EDC35. In *Proceedings of the 9th International Symposium on Detonation*, pages 831–841. Office of Naval Research, 1989.

6. Jensen, B. , Holtkamp, D. , and Rigg, P. . Accuracy Limits and Window Corrections for Photon Doppler Velocimetry. *Journal of Applied Physics*, 101:013523, 2007.

7. Sharpe, G. and Bdzil, J. . Interactions of Inert Confiners with Explosives. *Journal of Engineering Mathematics*, 54:273–298, 2006.